Carbohydrate Research 563 (2026) 109872

Contents lists available at ScienceDirect

Carbohydrate Research

journal homepage: www.elsevier.com/locate/carres

Influence of *N*- and *O*-glycosylation on structural properties and biological activity of a C-terminal LL-37 fragment

Daria Grzywacz [a], Francesca Nuti [b], Krzysztof Żamojć [a], Sergey A. Samsonov [a], Marcelina Malinowska [c], Małgorzata Paduszyńska [d], Anna Maria Papini [b], Joanna Makowska [a,*]

[a] Faculty of Chemistry, University of Gdańsk, Wita Stwosza 63, Gdańsk, 80-308, Poland
[b] Interdepartmental Research Unit of Peptide and Protein Chemistry and Biology, Department of Chemistry "Ugo Schiff", University of Florence, Via della Lastruccia 13, Sesto Fiorentino, 50019, Italy
[c] Faculty of Biology, Department of Medical Biology and Genetics, University of Gdańsk, Wita Stwosza 59, Gdańsk, 80-308, Poland
[d] Department of Pharmacy, Medical University of Gdańsk, Hallera 107, Gdańsk, 80-416, Poland

ARTICLE INFO

Keywords:
hCAP
Glycopeptide
Carbohydrate conjugation
LL-37 peptide
gAMP
Metal ion binding
Molecular dynamics

ABSTRACT

Glycosylation represents a versatile strategy in peptide glycoengineering to modulate the structural, physicochemical, and biological properties of antimicrobial peptides (AMPs). In this study, we report the synthesis and characterization of *O*- and *N*-glycosylated analogues of the C-terminal fragment of human cathelicidin LL-37 (Ac-DFLRNLVPRTES-COOH), achieved *via* solid-phase peptide synthesis using Fmoc-Thr(β-D-Glc) and Fmoc-Asn(β-D-Glc) as glycosylated building blocks. The metal-binding affinity of these glycopeptides (**N163** and **T168**) and the unmodified reference peptide (**hCAP**) toward Cu^{2+} and Mn^{2+} ions were evaluated by steady-state fluorescence spectroscopy. All peptides formed non-permanent complexes (K_a = 10^2 -10^4 M^{-1}), with the native **hCAP** exhibiting the highest affinity. Molecular dynamics (MD) simulations revealed that glycosylation reduced conformational flexibility without significantly altering the overall shape of the peptide. Occasional sugar-metal contacts were observed, indicating transient carbohydrate participation in metal coordination. Cytotoxicity studies using the MTT (3-[4,5-dimethylthiazol-2-yl]-2,5-diphenyltetrazolium bromide) assays confirmed the biocompatibility of all tested peptides, showing low toxicity against human fibroblasts, keratinocytes, and T-cells up to 100 μM. Our results demonstrate that carbohydrate conjugation subtly reshapes peptide-metal ion interactions, and structural dynamics. In this study, glycosylation serves primarily as a chemical model of post-translational modification, designed to probe how the presence of a carbohydrate moiety influences peptide conformation and coordination behaviour, rather than a strategy for enhancing antimicrobial function.

1. Introduction

The growing prevalence of drug-resistant bacterial strains has made the search for novel antimicrobial agents an urgent global priority, underscoring the need to identify new compounds with mechanisms of action to which bacteria have not yet developed resistance.

Among the promising alternatives are antimicrobial peptides (AMPs), which are relied upon as a novel class of therapeutics aimed at conquering drug-resistant bacteria and fungi [1–3]. AMPs represent an evolutionarily component of innate immunity, acting as the first line of defense against a wide spectrum of microbial pathogens in both humans and animals. Beyond their direct antimicrobial properties, AMPs modulate immune responses, wound healing, and inflammation, highlighting their potential as therapeutic agents and alternatives to conventional antibiotics [4]. Numerous synthetic AMPs are currently undergoing clinical trials for the treatment of a range of diseases, including diabetic foot ulcers or chemotherapy-associated infections [5,6]. However, their clinical application is frequently limited by low metabolic stability and rapid degradation by proteases under physiological conditions. Consequently, the strategies such as the incorporation of non-natural amino acids or peptidomimetics have been employed to address this issue [7–9].

This article is part of a special issue entitled: EUROCARB 2025 published in Carbohydrate Research.

* Corresponding author.
E-mail address: joanna.makowska@ug.edu.pl (J. Makowska).

https://doi.org/10.1016/j.carres.2026.109872
Received 13 November 2025; Received in revised form 18 February 2026; Accepted 23 February 2026
Available online 28 February 2026

There are numerous ways in which AMPs might interact with pathogens, including membrane disruption, generation of reactive oxygen species (ROS) [10], inhibition of cell wall synthesis [11], nucleic acid [12] and protein synthesis or by the withdrawal of essential metal ions. Given the current knowledge on this topic, researchers are exploring various strategies to enhance the antibacterial properties of peptide-based compounds [13,14].

One such strategy involves the glycosylation of AMPs (gAMPs), in which carbohydrate moieties are covalently attached to the side chain of the corresponding amino acid AMP peptide, most commonly serine, threonine, or asparagine [15]. Glycosylation is an effective chemical strategy to improve peptide stability. It enhances resistance to proteolytic degradation by proteases and enzymes in the biological environment. This action significantly prolongs the peptide's half-life *in vivo* [16]. Additionally, the introduction of hydrophilic sugar residues allows for the modulation of AMP hydrophilicity and conformational flexibility. This reduces the tendency for aggregation and potentially broadens their spectrum of biological activity [9,17]. gAMPs offer new tools to combat rising antimicrobial resistance to traditional medication, and are effective at low concentrations against a broad spectrum of pathogens [18,19].

Several studies have explored the impact of glycosylation, particularly *N*-linked glycosylation, on peptide properties including increased rigidity [20], solubility [21], propensity to aggregate [21], conformational changes to secondary structure of peptides [22], and their ability to influence interactions with neighboring peptides [23]. Notably, this last trait effectively allows glycopeptides to adopt chaperone-like qualities, and has been implicated as having a protective role in preventing fibril formation that contributes to amyloid diseases [22].

The second strategy to improve properties of AMPs involves combining them with metal ions, particularly those that are biologically active. Biologically indispensable metal ions exhibit a dual effect on the activity on antimicrobial peptides activity. Firstly, AMPs can bind these ions, thereby sequestering metals essential for microbial life and virulence (a mechanism known as nutritional immunity) [24]. Secondly, the metal ion itself can act as a booster for the AMP's antimicrobial activity by influencing its charge and/or structure [25]. Metal ions such as Zn^{2+}, Cu^{2+}, and Fe^{2+} can also play a crucial role [26]. Combining peptides with these ions can either enhance the peptide's inherent activity by affecting its charge and structure, or deprive bacteria of essential metals, thus inhibiting their growth [27].

Human cathelicidin antimicrobial peptide (hCAP18) is a multifunctional host-defense protein. It is expressed in various epithelial and immune tissues, where it contributes to the innate immune response through direct antimicrobial activity, immune cell chemotaxis, and modulation of inflammatory processes [28]. Upon proteolytic activation by proteinase 3, hCAP18 is cleaved to release the active peptide LL-37 [hCAP(134–170)]. LL-37 is an amphipathic, α-helical peptide composed of 37 amino acids. It displays broad-spectrum of antibacterial, antifungal, antiviral, and immunomodulatory properties [29–31].

In the present study, we examined the C-terminal 12-amino acid fragment of LL-37 (Ac-DFLRNLVPRTES-COOH), which remains comparatively underexplored in contrast to the extensively characterized shorter LL-37-derived peptides such as KR-12, FK-12, FK-16, or LL-25 [32]. Most structure-activity studies have focused on the *N*-terminal and central fragments of LL-37, which retain strong antimicrobial activity and well-defined amphipathic helices [33–35]. The C-terminal domain, however, has received less attention. Evidence indicates that this region may anchor membranes and neutralize LPS activities [36,37]. This region contains charged and polar residues (Asp159, Glu169, Thr168, Ser170) that might serve as potential coordination or modification sites, making it an attractive model for studying chemical derivatization.

This work is based on the foundational insights from previous studies on full-length LL-37 and its shortened analogues, particularly regarding metal ion coordination and conformational flexibility [38,39]. Earlier studies demonstrated that the full-length peptide forms labile but measurable complexes with Cu^{2+} and Zn^{2+} ions. While those studies highlighted the role of specific amino acid side chains in metal binding, the current work investigates how the introduction of sugar residues influences the peptide's metal-binding properties and structural behavior. Using spectroscopic techniques, we evaluated the binding affinity of glycosylated LL-37 fragments for selected metal ions, specifically Cu^{2+} and Mn^{2+}. This metal ions were selected because of their biological relevance and complementary coordination properties: Cu^{2+} often forms relatively strong, partly ligand-field governed complexes, whereas Mn^{2+} is more labile and typically interacts preferentially with oxygen donors. Complementary to the experiments, MD (molecular dynamics) based rigorous analysis was performed to estimate the influence of the glycosylation on the dominant conformation of the C-terminal fragment of LL-37 and to provide atomistic models of its complexes with selected metal ions for establishing the structure-functional relationship in this molecular system. Finally, biological assays were performed to assess the cytotoxicity and antimicrobial activity of the synthesized glycopeptides.

2. Results and discussion

2.1. Synthesis

In this study, we designed and synthesized three peptide variants derived from the C-terminal fragment of the LL-37 peptide (DFLRNLVPRTES). All peptides were N-terminally acetylated and contained a free C-terminal carboxylic acid group. This modification strategy reflects the natural chemical termini of the fragment within the full-length LL-37 sequence in hCAP18, where the N-terminus is blocked as a result of proteolytic processing and the C-terminus remains unamidated. The first one was the unmodified reference peptide hCAP(159-170) (referred as **hCAP**, Fig. 1), while the remaining two were glycopeptides containing a single β-D-glucose unit covalently attached to selected amino acid residues. In N163(Glc)hCAP(159–170) (referred to as **N163**, Fig. 2), *N*-glycosylation was introduced at the asparagine residue (Asn163), while in T168(Glc)hCAP(159–170) (referred to as **T168**, Fig. 3), *O*-glycosylation was introduced at the threonine residue (Thr168). This strategy allowed a direct comparison of the impact of glycosylation at different sites and through different linkage types (*N*- vs. *O*-linked). Glycosylation of the C-terminal Ser170 was not pursued because this part of the terminal region contributes to maintaining the native structural integrity and physicochemical properties of the peptide, including its interactions with membranes and metal ions [40].

The synthesis of the glycosylated building blocks was conducted manually. For Fmoc-L-Thr(β-D-Glc(Ac)$_4$)-OH, per-*O*-acetylated glucose was coupled to Fmoc-L-Thr-OH in the presence of $SnCl_4$ as a Lewis acid promoter. The reaction was carried out under an argon atmosphere in anhydrous acetonitrile at room temperature, proceeding smoothly in a single step with a 55% yield. The β-configuration of the glycosidic bond was confirmed by ^{1}H NMR, with a characteristic coupling constant of $J = 7.93$ Hz for the anomeric proton.

The synthesis of Fmoc-L-Asn(β-D-Glc(Ac)$_4$)-OH was carried out in several steps using a glycosylamine-based approach. In this strategy, a glycosylamine derivative was reacted with Fmoc-L-Asp-O*t*Bu in the presence of NMM and DMT-NMM·BF_4 under microwave irradiation, as described in the literature [41]. Following deprotection of the C-terminal *tert*-butyl ester, the Fmoc-protected glycoamino acid was obtained, suitable for incorporation into peptides *via* solid-phase synthesis.

All building blocks were compatible with Fmoc/*t*Bu SPPS chemistry and were successfully incorporated into peptide sequences. Comprehensive information on the synthesis and characterization of the glycopeptides is presented in the Materials and Methods section and in the Supporting Information. The identity and purity of the final products were confirmed by electrospray ionization mass spectrometry (ESI-MS) and MALDI-TOF MS. Retention times observed in HPLC analyses

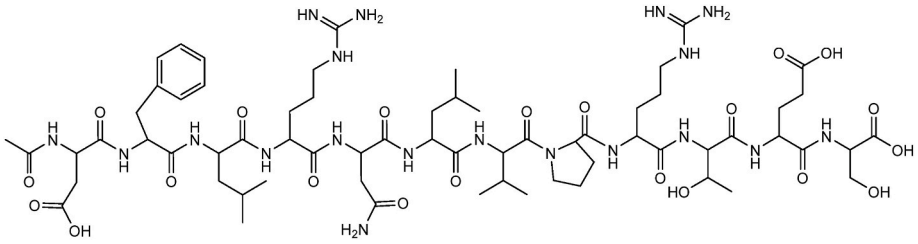

Fig. 1. Chemical structure of peptide **hCAP**.

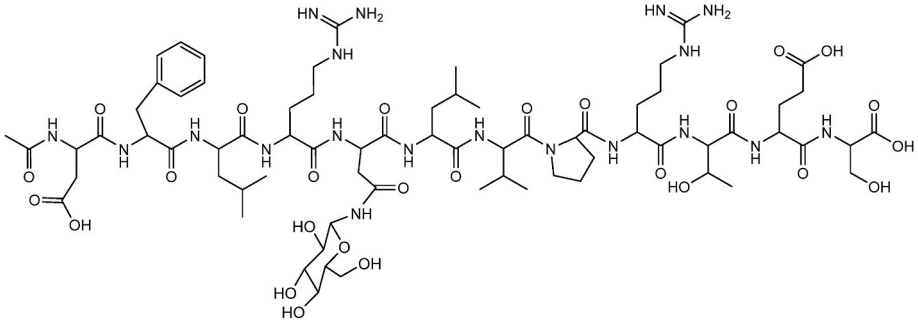

Fig. 2. Chemical structure of **N163**.

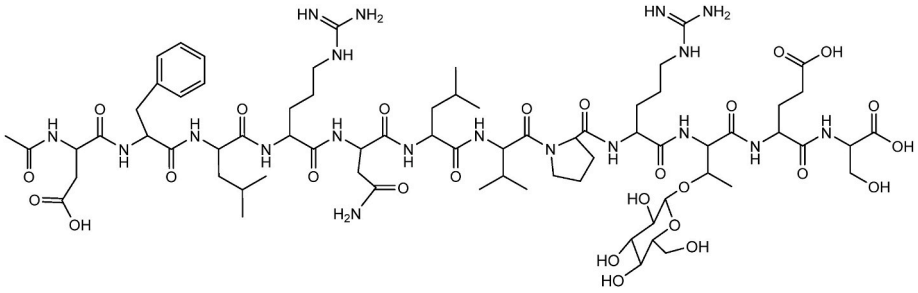

Fig. 3. Chemical structure of **T168**.

indicated increased hydrophilicity of the glycosylated peptides, consistent with the addition of a sugar moiety (Table 1).

2.2. Fluorescence spectroscopy

The binding (association) constants (K_A) of the newly formed complexes were determined by the equation: $\frac{1}{F_0-F} = \frac{1}{F_0} + \frac{1}{K_A F_0[Q]}$ [42], where F_0 and F are the fluorescence intensities in the absence and in the presence of quencher at concentration [Q]. According to that, appropriate plots were constructed for all investigated peptide/metal ion systems based on the relationship of $\frac{F_0}{F_0-F}$ vs. $\frac{1}{[Q]}$ (Fig. 4). From the regression equations applied for these curves, binding constant values were obtained (as the average of two independent experiments) and are gathered as the inset in Fig. 4. It can be concluded that steady-state fluorescence spectroscopy revealed weak binding of Cu^{2+} and Mn^{2+} to all synthesized peptides: **hCAP**, **N163**, and **T168** (binding constant values ranging from 10^2 to 10^4 M^{-1}). Nevertheless, by comparing the obtained binding constants, it is clear that Cu^{2+} ions form more stable complexes with all studied peptides than Mn^{2+} (one order of magnitude). Additionally, spectrofluorometric titrations performed at different biologically relevant pH values (5.5–7.4) showed a moderate pH dependence of Cu^{2+} binding strength, with the affinity increasing gradually at higher pH, while preserving most likely the same coordination pattern (Fig. S10 in Supplementary Information).

Furthermore, the binding of both ions to **hCAP** (peptide without a modification caused by the presence of a sugar moiety) is stronger when compared to its glycosylated counterparts **N163** and **T168**. An increase in molecular size and polarity, along with a shift to a less-planar structure, might explain the observed phenomenon – steric hindrance can happen when a sugar moiety substitutes the hydrogen atom in amide or hydroxyl group, which may limit metal ion access to key coordinating residues and reduce the affinity of Cu^{2+} and Mn^{2+} for the modified peptide. An alternative theory is that glycosylation makes peptide less

Table 1
Characterization of synthesized peptides.

Peptide abbreviation		Sequence	Modification	Calculated $[M+H]^+$ (Da)	Observed $[M+2H]^{2+}$ (Da)	Rt (min)[a]
hCAP	hCAP(159-170)	Ac-DFLRNLVPRTES-COOH	None	1489.7	1490.4	4.55
N163	N163(Glc)hCAP(159-170)	Ac-DFLRN(D-Glc)LVPRTES-COOH	*N*-glycosylation (β-D-Glc)	1651.8	1652.3	4.35
T168	T168(Glc)hCAP(159-170)	Ac-DFLRNLVPRT(D-Glc)ES-COOH	*O*-glycosylation (β-D-Glc)	1651.8	1652.4	4.18

[a] Analytical HPLC gradient: 10-90% B in 5 min a 0.6 mL/min at 35 °C.

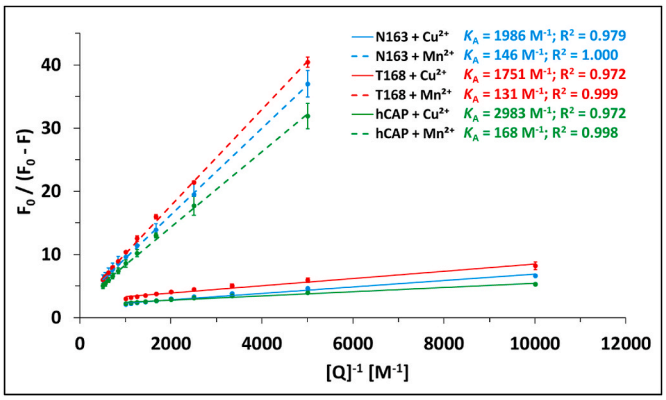

Fig. 4. The plots of $\frac{F_0}{F_0-F}$ as a function of $[Q]^{-1}$ for the steady-state fluorescence quenching of **N163**, **T168**, and **hCAP** by Cu^{2+} and Mn^{2+} in 10 mM MES buffer of pH 6.0; λ_{ex} = 260 nm; λ_{em} = 284 nm; 298.15 K.

hydrophobic, meanwhile hydrophobic interactions are essential for small particle binding to proteins or peptides. Structural modification of the peptide by the attached sugar unit could be another explanation for this phenomenon. In fact, the minor variations in the relative orientation of the aromatic rings due to the attached sugar moieties, which influence the binding specificity and affinity, have been noted before for various glycosylated derivatives of a specific aromatic pharmacophore [43]. However, in order to confirm the mechanism responsible for the reduced metal affinity after glycosylation, molecular dynamics simulations were performed.

2.3. Molecular modeling

MD simulations were performed to obtain atomistic models of the studied systems that could potentially contribute to the qualitative understanding of the experimental data. The introduction of the glucose residue into the peptide slightly restricts its movements, rendering the MD-obtained structural ensemble less flexible (Fig. 5). At the same time, the shape of the molecule is not significantly affected. Because reliable high-quality parameters for Cu^{2+} are lacking in the AMBER package [44], we restricted our simulations to Mn^{2+}, for which well-established parameters are available. When a Mn^{2+} ion is added to the peptide, it is predominantly coordinated by its C-terminal carboxyl group and the carboxyl group of Glu169 for all peptides. In case of **T168**, the glucose residue also participates in the coordination of the ion (Fig. 6).

2.4. Biological studies

To evaluate the cytotoxicity of the peptides **hCAP**, **N163**, and **T168**, we assessed the metabolic activity of human dermal fibroblasts (HDFa), keratinocytes (HaCaT), and T lymphocytes (Jurkat) after 24 h exposure to peptide concentrations ranging from 1.52 to 100 μM using the MTT assay.

Across all tested concentrations, none of the peptides induced a statistically significant reduction in cell viability in any of the cell lines. Cell viability remained consistently above 70% even at the highest concentration tested, with only slight, non-significant decreases observed in a dose-dependent manner. These findings indicate that **hCAP**, **N163**, and **T168** do not exert cytotoxic effects on fibroblasts, keratinocytes, or lymphocytes under the tested conditions (Fig. 7).

Additionally, antimicrobial activity assays were conducted against selected Gram-positive and Gram-negative bacteria, as well as fungal strains. The tested peptides did not inhibit growth of any of the reference strains at the maximal tested concentration (512 μg/mL); therefore MIC >512 μg/mL for all peptides under the conditions used (Table 2). The experimental details are provided in the *Materials and Methods* section.

Truncation of LL-37 to its C-terminal 12-residue fragment resulted in the loss of antimicrobial activity. Furthermore, antimicrobial testing indicated that glycosylation did not restore or enhance the peptide's activity. Because neither the native peptide nor its glycosylated analogues exhibited antimicrobial activity under metal-free conditions, further biological assays in the presence of Cu^{2+} or Mn^{2+} were not pursued. Although glycosylation can improve solubility and proteolytic stability, it can also hinder antimicrobial peptides' ability to interact with membranes [45]. In short peptide fragments that rely on amphipathicity and surface activity, the attachment of a sugar moiety may disrupt the amphipathic balance, sterically hinder its approach to the bacterial membrane, and/or prevent the optimal insertion or aggregation required for membrane disruption. Similar observations have been reported in recent studies, where glycosylation improved peptide stability but led to only marginal or negligible increases in antimicrobial potency [9,46].

3. Conclusion

This study examined site-specific glycosylation effects on the structure and metal-binding properties of a C-terminal LL-37 fragment. Two glycosylated analogues were synthesized: **T168**, modified at a threonine residue *via O*-glycosylation, and **N163**, modified at an asparagine residue *via N*-glycosylation. The study focused specifically on how these modifications impact metal binding, conformational changes, and antimicrobial activity.

Fluorescence spectroscopy showed that all peptides exhibited weak and reversible (dynamic) interactions with Cu^{2+} and Mn^{2+} ions. Among them, the reference peptide showed the highest, though still weak, affinity for both metal ions. Theoretical studies supported these observations. All peptides bind metal ions in a similar manner, mainly through coordination to the C-terminal carboxyl group and the side-chain carboxyl group of Glu169.

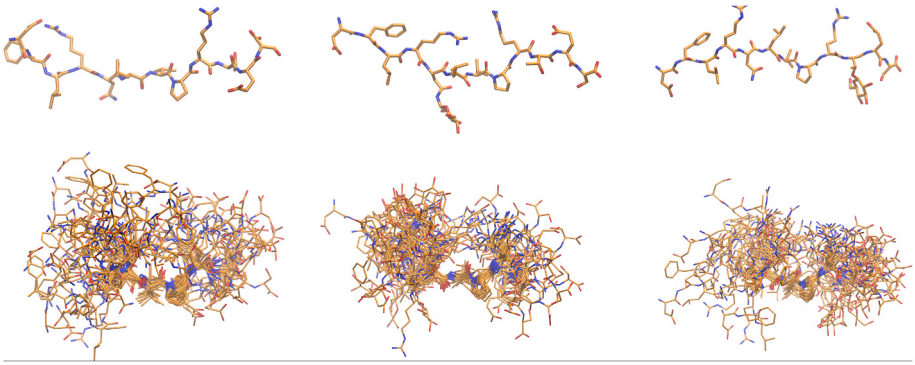

Fig. 5. MD-based analysis of **hCAP** (left), **N163** (middle) and **T168** (right). Top panel: starting structures of the peptides; bottom panel: corresponding structural ensemble obtained in the 1 μs MD simulation (50 equidistantly distributed frames). Peptides are rendered in sticks.

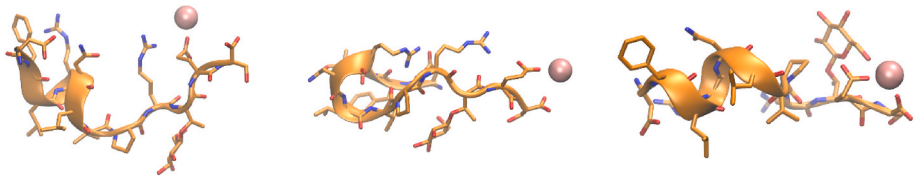

Fig. 6. MD-based analysis T168 in the presence of Mn^{2+} ion. Three representative binding modes are shown. Peptides are rendered in sticks and cartoon, the Mn^{2+} ion is shown as a sphere.

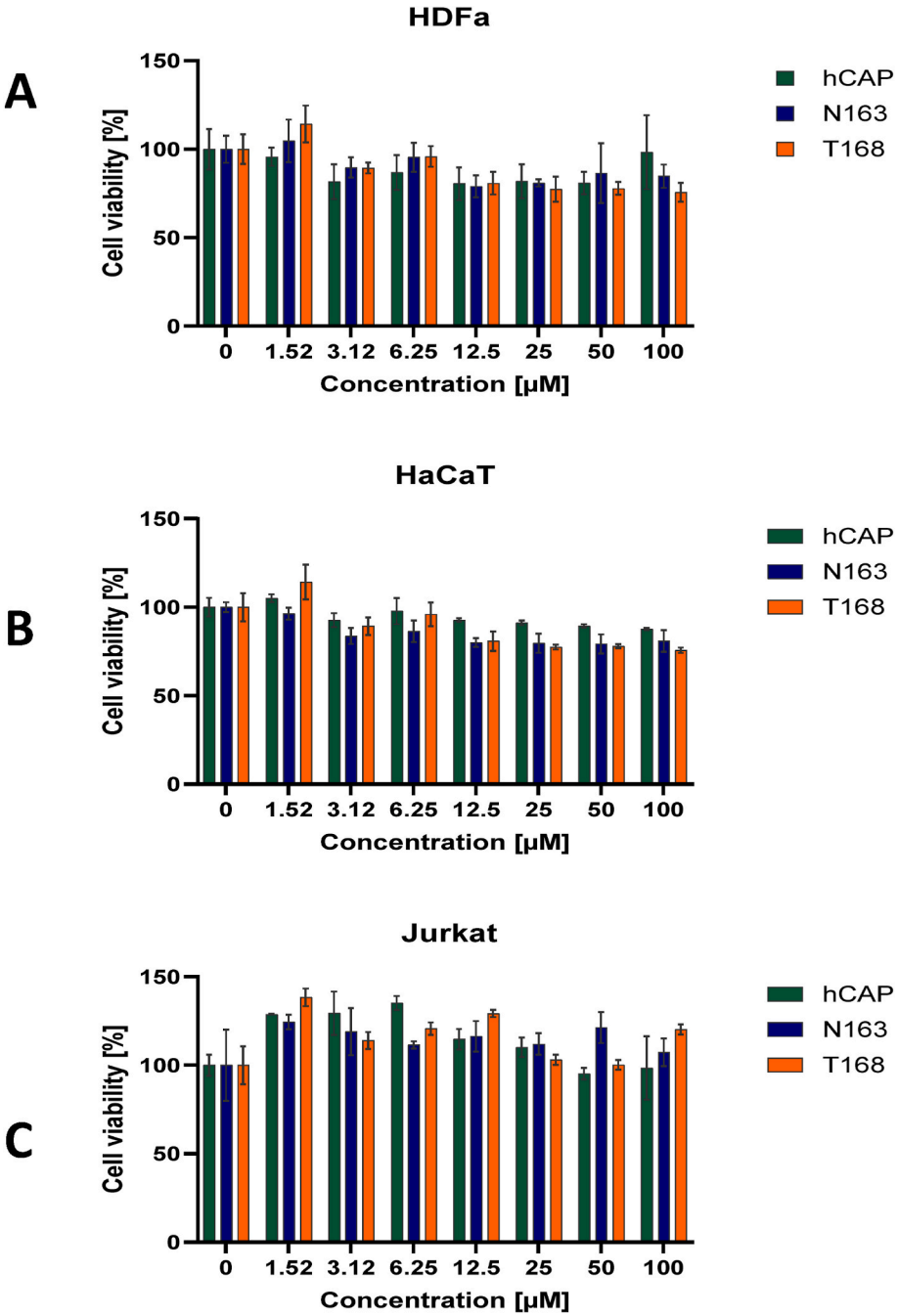

Fig. 7. Cytotoxicity of peptides **hCAP**, **N163**, and **T168**. Cell viability was assessed after 24 h of exposure to adult human dermal fibroblasts (**A** – HDFa), keratinocytes (**B** – HaCaT), and immortalized T-cells (**C** – Jurkat) across a concentration range of 1.52 to 100 μM. Data are presented as mean ± standard deviation from three independent replicates. No statistically significant differences were observed compared to untreated cells (0 μM), as determined by one-way ANOVA followed by Tukey–Kramer HSD post hoc test ($p < 0.05$).

From a structural viewpoint, the introduction of a carbohydrate residue increases the hydrophilic surface area and modifies the local

Table 2
Antimicrobial activity (MIC [μg/mL]) of peptides against planktonic cells.

Peptide	Gram-negative bacteria			Gram-positive bacteria			Fungi		
	E. faecium ATC 700221	*S. aureus* ATCC 6538	*S. aureus* ATCC 25923	*E. coli* ATCC 25922	*K. pneumoniae* ATCC 700603	*A. baumanii* ATCC 19606	*A. brasiliensis* ATC 16404	*C. albicans* ATCC 10231	*C. lypolytica* PCM 2680
hCAP	>512	>512	>512	>512	>512	>512	>512	>512	>512
N163	>512	>512	>512	>512	>512	>512	>512	>512	>512
T168	>512	>512	>512	>512	>512	>512	>512	>512	>512

electrostatic potential of the peptide environment, thereby affecting ion approach and complex stability. Molecular dynamics simulations further supported this interpretation, showing that glucose addition restricts conformational flexibility and occasionally introduces transient carbohydrate-metal contacts without altering the dominant carboxylate-based coordination. These findings indicate that glycosylation indirectly affects metal binding by subtly altering hydration and charge patterns, rather than creating new strong binding sites.

Glycosylation, whether on **Asn163** (*N*-linked) or **Thr168** (*O*-linked), was found to reduce conformational flexibility, with the stiffening effect being most pronounced in the **N163** analogue. Molecular dynamics simulations revealed a narrower structural ensemble due to restricted backbone mobility, likely caused by steric constraints imposed by the sugar ring and intramolecular hydrogen bonding between the carbohydrate and neighboring residues. In the **T168** analogue, the glucose moiety occasionally approached the Mn^{2+} ion and formed weak, geometry-dependent coordination contacts, suggesting a transient yet cooperative carbohydrate–metal interaction.

While steady-state fluorescence experiments demonstrate an overall reduction in metal affinity upon glycosylation, MD snapshots (Fig. 6) reveal that such sugar-assisted coordination represents a minor binding mode, occurring only when the pyranose ring is favorably oriented toward the metal ion. Thus, occasional participation of the carbohydrate moiety may locally stabilize specific conformations but does not compensate for the overall loss of affinity caused by steric hindrance and reduced accessibility of canonical coordinating groups.

The correlation between peptide structure and divalent cation binding was explored to determine whether glycosylation modulates metal-ligand interactions that could influence biological properties. Although LL-37 and its fragments lack canonical metal-binding motifs such as ATCUN (H_2N–X–X–His), HExxH, or DxDxE sequences, the C-terminal fragment DFLRNLVPRTES retains potential coordination sites, including the side-chain carboxylates of Asp159 and Glu169 as well as the free terminal carboxyl group. These residues are known to weakly interact with divalent cations such as Cu^{2+} and Mn^{2+} through electrostatic or monodentate coordination [47,48].

This study focused on metal binding in the shortened, glycosylated fragment. Increasing evidence suggests that metal ions can influence the activity, stability, and folding of antimicrobial and glycopeptide systems, even in the absence of typical canonical motifs. In particular, Cu^{2+} and Mn^{2+} play key roles in host defense, redox balance, and stress responses. Their interactions with AMPs and glycosylated forms may alter peptide membrane association and aggregation [17,49]. Consequently, studying how glycosylation modifies weak, transient peptide–metal interactions provides insight into ways sugars can affect AMP structure and function.

Cytotoxicity assays confirmed that all tested peptides were non-toxic to human cell lines (HDFa, HaCaT, Jurkat), with cell viability remaining above 70% at all tested concentrations. This result highlights that glycosylation can stabilize peptides. This is consistent with established findings that glycosylation enhances solubility, serum stability, and resistance to proteolytic degradation. The attached carbohydrate residues increase the hydration shell and reduce nonspecific membrane interactions, contributing to the observed low cytotoxicity.

The truncated LL-37 fragment used in this study was found to be biologically inactive at concentrations up to 512 mg/L. This result indicates that the short C-terminal segment does not retain the full peptide's antimicrobial properties. This observation is consistent with previous reports showing that antimicrobial activity in LL-37 is primarily associated with the central and N-terminal amphipathic regions (e.g. KR-12, FK-16) [33–35]. Consequently, the present results should be interpreter as a glyco-structural investigation, into how carbohydrate conjugation influences peptide conformation, flexibility, and metal binding in a biologically relevant yet non-active fragment of LL-37.

4. Materials and methods

4.1. Synthesis

4.1.1. General procedure for synthesis glycosylated building blocks

All solvents and chemical reagents were obtained from commercial suppliers without additional purification. Nuclear Magnetic Resonance (NMR) spectra for ^1H and ^{13}C were acquired using a Bruker Avance III spectrometer operating at 500.13 MHz and 125.76 MHz, respectively. Mass spectra in positive-ion mode were recorded on a Bruker Biflex III MALDI-TOF spectrometer. Thin-layer chromatography (TLC) was conducted on aluminum sheets coated with E. Merck Kieselgel 60 F_{254} silica gel. Detection of compounds on the TLC plates was achieved by spraying with 1% sulfuric acid in methanol, followed by heating to approximately 200 °C in a stream of hot air, as well as by ultraviolet (UV) illumination. Flash column chromatography was carried out on a PuriFlash 450 system equipped with a UV-DAD detector.

4.1.2. N^{α}-(9-Fluoroenylmethoxycarbonyl)-O-(2,3,4,6-tetra-O-acetyl-β-D-glucopyranosyl)-L-threonine [N^{α}-Fmoc-L-Thr(β-D-Glc(Ac)$_4$)-OH]

The glycosylated amino acid was synthesized using a modified version of the procedure described by Salvador et al. [50].

Per-*O*-acetylated glucose (1.0 g; 2.55 mmol) and Fmoc-L-Thr-OH (0.87 g; 2.55 mmol) were dissolved in dry acetonitrile (10 mL) in a round-bottom flask containing freshly dried, ground 4 Å molecular sieves. The reaction was carried out in a flask equipped with a Schlenk line. After the addition of $SnCl_4$ (400 μL; 3.3 mmol), the reaction mixture was thoroughly degassed by three freeze-pump-thaw cycles under an argon atmosphere. After the final cycle, the flask was filled with argon, and the reaction was carried out overnight at room temperature. The reaction progress was monitored by TLC (chloroform/methanol, *v/v*, 11:1). Upon completion, the reaction mixture was passed through a silica gel column using CH_2Cl_2 as an eluent. The organic layer was washed successively with saturated $NaHCO_3$ solution (2 × 20 mL), brine (20 mL), and then dried over $MgSO_4$. The solvent was evaporated, and the residue was purified by flash chromatography (chloroform/methanol, *v/v*, 20:1). In this way, a white solid N^{α}-Fmoc-L-Thr(β-D-Glc(Ac)$_4$)-OH was obtained (0.94 g; 55%); ^1H NMR (500 MHz, $CDCl_3$-*d*) δ ppm: 1.23 (d, $J = 6.26$ Hz, 3 H, CH_3), 2.02 (s, 3 H), 2.05 (s, 6 H), 2.13 (s, 3 H), 3.65 (dd, $J = 9.77$, 2.90, 1 H, H-5), 4.06 (dd, $J = 12.36$, 3.74 Hz, 1 H, H-6), 4.26 (t, $J = 7.17$ Hz, 1 H, Fmoc-CH), 4.35 - 4.45 (m, 5 H), 4.49 (dd, $J = 12.36$, 2.29 Hz, 1 H, H-6'), 4.54 (d, $J = 7.93$ Hz, 1 H, H-1), 4.95 (t, $J = 9.31$ Hz, 1 H), 5.10 (t, $J = 9.77$ Hz, m, 1 H), 5.19 (t, $J = 9.46$ Hz, 1 H, H-3), 5.63 (d, $J = 9.31$ Hz, 1 H, NH), 7.32 (t, $J = 7.48$ Hz, 2 H), 7.40 (t, $J = 7.40$ Hz, 2 H), 7.63 (t, $J = 7.32$ Hz, 2 H), 7.76 (d, $J = 7.48$ Hz, 2 H); ^{13}C NMR (126 MHz, $CDCl_3$-*d*) δ ppm 17.61, 20.61, 21.00, 47.12, 58.03, 61.27, 67.44, 68.38, 71.11, 71.77, 72.59, 76.42, 76.78, 77.03, 77.28,

99.85, 119.98, 125.24, 127.10, 127.14, 127.74, 141.29, 143.73, 143.87, 156.80, 169.25, 169.40, 170.32, 171.47, 172.26; MALDI-TOF-MS: *m/z* calcd for $C_{33}H_{37}NO_{14}$ 671.43, found 694.138 $(M + Na)^+$, 710.117 $(M + K)^+$.

4.1.3. N^{α}-(9-Fluoroenylmethoxycarbonyl)-O-(2,3,4,6-tetra-O-acetyl-β-D-glucopyranosyl)-L-asparagine [Fmoc-L-Asn(β-D-Glc(Ac)$_4$)-OH]

Fmoc-L-Asn(β-D-Glc(Ac)$_4$)-OH was synthesized according to a previously described procedure [41].

4.1.4. General procedure for peptide synthesis and purification

Peptides were synthesized using a combination of manual methods and microwave-assisted solid-phase synthesis (MW-SPPS) automated synthesis on a Liberty Blue™ 2.0 (CEM Corporation, Matthews, NC, USA) peptide synthesizer, following standard Fmoc/*t*Bu solid-phase peptide synthesis protocols on TentaGel resin.

The MW-SPPS protocol was reported previously [51,52]. The synthesis involved iterative cycles of Fmoc deprotection and amino acid coupling. In manual steps, Fmoc groups were removed by treating the resin with 20% (*v/v*) piperidine in *N,N*-dimethylformamide (DMF) for 10 min at room temperature. After deprotection, the resin was thoroughly washed with DMF and dichloromethane (DCM) to remove residual reagents. Coupling reactions, for standard amino acids, were performed using a threefold molar excess of Fmoc-protected amino acids, activated with *N,N'*-diisopropylcarbodiimide (DIC) and either 1-hydroxybenzotriazole (HOBt) or OxymaPure. The reactions proceeded in a DMF/DCM mixture for 1 h at room temperature. The progress of each coupling and deprotection step was monitored using the chloranil test. N-terminal acetylation was achieved as a final capping step by adding acetic anhydride in DMF.

Upon completion of the peptide assembly, the final deprotection and cleavage from the resin were achieved by treating the resin with a cleavage cocktail composed of trifluoroacetic acid (TFA), triisopropylsilane (TIS), and water, in 95:2.5:2.5 (*v/v/v*) ratio. This step simultaneously removed side-chain protecting groups and released the peptide from the resin. The crude peptides were precipitated by the addition of cold diethyl ether, collected by centrifugation, and lyophilized.

Purification of selected peptides was performed by reverse-phase high-performance liquid chromatography (RP-HPLC). Peptide identity was confirmed by mass spectrometry techniques such as electrospray ionization (ESI-MS) on a Single Quadrupole ESI-MS Micromass ZQ system coupled to a Waters Alliance 2695 RP-HPLC system (Waters, Milfors, Massachusetts, USA) and by matrix-assisted laser desorption/ionization time-of-flight (MALDI-TOF) mass spectrometry. All the RP-HPLC analyses were performed on a Waters Alliance 1695 Separation Module equipped with a Photodiode Array Detector Waters PAD 2996 (Waters, Milford Massachusetts, USA) using a BIOshell™ A160 Column C18 (2.7 μm, 3 × 100 mm) at 35 °C. Analytical HPLC gradient was run at a flow rate of 0.6 mL/min: 10-90% of B in 5 min. The solvents systems: A (0.1% TFA in H_2O) and B (0.1% TFA in CH_3CN).

4.1.5. Synthesis of glycosylated peptides

Glycopeptides were synthesized by MW-SPPS following the Fmoc/*t*Bu strategy, using the Liberty Blue™ automated microwave peptide synthesizer (CEM Corporation, Matthews, NC, USA). The synthesis proceeded on the synthesizer up to the incorporation of glycosylated amino acids N^{α}-Fmoc-L-Thr(β-D-Glc(Ac)$_4$)-OH or N^{α}-Fmoc-L-Asn(β-D-Glc(Ac)$_4$)-OH. Both glycosylated building blocks, as well as all remaining amino acid residues, were coupled manually to ensure optimal control of the reaction conditions and to maximize coupling efficiency. Couplings were performed using HBTU/HOBt as activating agents in the presence of DIPEA in DMF. The progress of the reaction was monitored by the chloranil test. After completion of the peptide sequence, cleavage from the resin was carried out using a standard TFA cleavage cocktail.

O-deacetylation of the glycan moieties was performed according to a protocol based on Sikora et al. [53]. The lyophilized crude glycopeptide was dissolved in dry methanol (2 mL), and a 0.1 M solution of sodium methoxide in methanol was added dropwise until the pH reached approximately 10. The reaction mixture was stirred for 15–30 min. The reaction was then quenched by the addition of solid CO_2, leading to neutralization of the solution. The solvent was removed under reduced pressure, and the crude product was purified by preparative reverse-phase HPLC.

4.2. Experiments concerning interactions with metal ions

4.2.1. Steady-state fluorescence spectroscopy (SF)

The Cary Eclipse Varian (Agilent, Santa Clara, CA, USA) spectrofluorometer equipped with a temperature controller and 1.0 cm multicell holder was used to perform all steady-state fluorescence spectroscopy experiments. All measurements were performed in 10 mM MES buffer (pH 6.0) at 298.15 K. The excitation wavelength was always set at 260 nm. The excitation and emission slit widths were fixed at 10 nm. All fluorescence intensity values have been corrected for the inner filter effect. In the fluorescence titration experiments (performed manually by using a micropipette), 2 mL of each peptide at a fixed concentration (c = 0.25 mM) was titrated by ten successive additions of 2 μL stock solutions of $Cu(NO_3)_2$ (c = 0.1 M) and $Mn(NO_3)_2$ (c = 0.2 M). After each addition, the mixture was shaken, and the fluorescence intensity value was recorded at least ten times. The fluorescence intensities of the band at 284 nm – corresponding to the initial maximum emission of phenylalanine – were used to calculate the binding constants. All spectrofluorometric experiments were performed twice; thus all obtained values are means from two independent experiments.

4.3. Molecular modeling

The structures of the peptides were built in xleap module of AMBER20 package [44] in the extended conformation and glucose residues were covalently added in case of N163 and T168 variants to the corresponding amino acid residues. MD simulations were performed with AMBER20 [44] with the ff14SB [54] and GLYCAM06 [55] force field parameters for the protein and carbohydrate parts, respectively. The periodic boundary conditions were used with a TIP3P octahedral water box with a layer of water molecules of 12 Å from the border of the periodic box to the solute. In case of the simulations with Mn^{2+} ion, the standard parameters available in AMBER20 [44] were used, and the ion was randomly placed in the box. To neutralize the system's net charge in the presence of Mn^{2+} ion, Cl^- counterions were used. Two steps of energy minimization were performed: first 500 cycles of steepest descent and 1000 conjugate gradient cycles with harmonic restraints of 10 kcal/mol/Å^2 on the solute, and then 3000 steepest descent and 3000 conjugate gradient cycles without restraints. Subsequently, the system was heated up to 300 K for 10 ps in the constant-temperature, constant-volume (NVT) ensemble, followed by the simulations in the constant-temperature, constant-pressure (NPT) ensemble at the pressure of 105 Pa until the density of solvent converged. Finally, 1 μs MD production run was performed in NPT ensemble. The time integration step was 2 fs, and the cutoff for non-bonded interactions 8 Å. The SHAKE algorithm for the covalent bonds including hydrogen atoms and the Particle Mesh Ewald procedure were used for long-range electrostatic calculations. Visualisation of the obtained trajectories was performed in VMD [56].

4.4. Biological study

4.4.1. Cell viability assay

Cell viability was assessed using the MTT [3-(4,5-dimethylthiazol-2-yl)-2,5-diphenyltetrazolium bromide] assay. Human dermal fibroblasts, adult (HDFa; ATCC® PCS-201-012™), immortalized human keratinocytes (HaCaT; CLS Cell Lines Service GmbH, Eppelheim, Germany), and

an immortalized T-lymphocyte cell line (Jurkat; ATCC® TIB-152™) were used in this study. HDFa and HaCaT cells were seeded at densities of 1×10^4 and 2×10^4 cells per well, respectively, in 96-well flat-bottom CELLSTAR® cell culture plates (Greiner Bio-One, Germany) containing 100 μL of growth medium (DMEM supplemented with 10% FBS and 1% Pen/Strep). Jurkat cells were seeded at a density of 1×10^5 cells per well in 96-well U-bottom CELLSTAR® plates in 100 μL of RPMI medium supplemented with 10% FBS and 1% Pen/Strep. Cells were incubated at 37 °C in a humidified atmosphere for 24 h. Cytotoxicity (MTT) assays were performed in cell culture media at pH ≈ 7.4.

After that time, the culture medium was replaced with fresh DMEM or RPMI containing the tested compounds, prepared in a concentration range using two-fold serial dilutions from 1.52 to 100 μM. Cells were then incubated for an additional 24 h under the same conditions. Following 24 h of exposure to the tested peptides, the culture medium for adherent cells was replaced with 100 μL of MTT reagent (1 mg/mL in RPMI-1640 medium; Sigma-Aldrich, St. Louis, MO, USA), and the cells were incubated for 3 h. For Jurkat cells, which are a suspension cell line, the culture plates were centrifuged for 5 min at 1000 rcf, after which the culture medium was replaced with RPMI medium containing MTT, and the cells were incubated for 3 h. The assay is based on the reduction of yellow tetrazole to purple formazan by metabolically active cells, serving as an indicator of cell viability.

After incubation, the medium was removed, and the insoluble formazan crystals were dissolved in 100 μL of dimethyl sulfoxide (DMSO; Sigma-Aldrich, St. Louis, MO, USA). The absorbance was read at 570/660 nm using a BioTek Synergy H1 Microplate Reader (Agilent, Santa Clara, USA). Cell viability was calculated relative to control cells (untreated cells, cultured only in growth medium) and presented as a percentage. One-way ANOVA followed by Tukey's post hoc test was performed to determine statistical significance ($p < 0.05$) using GraphPad Prism version 10.0.

4.4.2. Minimum inhibitory concentration (MIC) assay

Minimum inhibitory concentration (MIC) was determined with reference strains of gram-positive bacteria (*Enterococcus faecium* ATCC 700221, *Staphylococcus aureus* ATCC 6538, *S. aureus* ATCC 25923), gram-negative bacteria (*Acinetobacter baumanii* ATCC 19606, *Escherichia coli* ATCC 25922, *Klebsiella pneumoniae* ATCC 700603) and fungi (*Aspergillus brasiliensis* ATCC 16404, *Candida albicans* ATCC 10231, *C. lypolytica* PCM 2680). The reference strains were purchased from the Polish Academy of Sciences (Wroclaw, Poland).

MIC assays were performed on 96-well polystyrene plates with the dilution method in liquid media: Mueller-Hinton II broth (MHB II) for bacteria and Roswell Park Memorial Institute 1640 Medium (RPMI) for fungi at pH ≈ 7.4 according to CLSI guidelines.

The bacteria were cultured at 37 °C under aerobic conditions overnight in Brain-Heart Infusion broth (BHI) were centrifuged (2500 rpm, 10 min) and suspended in MHB II medium to inoculums of ca. 5×10^5 CFU/mL. The bacterial suspensions were exposed to the tested compounds (concentration range 1 – 512 μg/mL) for 24 h at 37 °C under aerobic conditions.

The *Candida* strains were cultured in a Sabouraud Dextrose Broth (DSB) for 48 h, under aerobic conditions at 25 °C and the cultures were centrifuged (2500 rpm, 10 min). *Aspergillus brasiliensis* was cultured on the Sabouraud Dextrose Agar (SDA) for 7 days at 25 °C under aerobic conditions and washed with 0.9% NaCl supplemented with Tween 20 (0.01%). The fungi were suspended in RPMI to inoculums of ca. 5×10^3 CFU/mL and exposed to the tested compounds (concentration range 1 – 512 μg/mL) for 48 h at 25 °C under aerobic conditions.

After incubation, the results were read visually by comparing to the negative (pure MHB II/RPMI) and positive (MHB II with bacteria/RPMI with fungi) controls. MIC is defined as the lowest concentration of the compound which inhibits the growth of microbes. The experiments were performed in triplicate.

Funding

This work was supported by *UGrant-advanced* Nr533-T000-GA-17-24 (University of Gdansk).

CRediT authorship contribution statement

Daria Grzywacz: Conceptualization, Data curation, Investigation, Methodology, Validation, Writing – original draft. **Francesca Nuti:** Investigation, Methodology. **Krzysztof Żamojć:** Data curation, Investigation, Methodology, Writing – review & editing. **Sergey A. Samsonov:** Data curation, Formal analysis, Investigation, Methodology. **Marcelina Malinowska:** Investigation, Methodology. **Małgorzata Paduszyńska:** Investigation, Methodology. **Anna Maria Papini:** Supervision, Writing – review & editing. **Joanna Makowska:** Conceptualization, Funding acquisition, Investigation, Project administration, Supervision, Writing – review & editing.

Declaration of competing interest

The authors declare that they have no known competing financial interests or personal relationships that could have appeared to influence the work reported in this paper.

Appendix A. Supplementary data

Supplementary data to this article can be found online at https://doi.org/10.1016/j.carres.2026.109872.

Data availability

Data will be made available on request.

References

[1] J.D. Steckbeck, B. Deslouches, R.C. Montelaro, Expet Opin. Biol. Ther. 14 (2014) 11–14, https://doi.org/10.1517/14712598.2013.844227.
[2] G. Annunziato, G. Costantino, Expert Opin. Ther. Pat. 30 (2020) 931–947, https://doi.org/10.1080/13543776.2020.1851679.
[3] M. Büyükkiraz, Z. Kesmen, J. Appl. Microbiol. 132 (2022) 1573–1596, https://doi.org/10.1111/jam.15314.
[4] N.G.O. Júnior, C.M. Souza, D.F. Buccini, M.H. Cardoso, O.L. Franco, Nat. Rev. Microbiol. 23 (2025) 687–700, https://doi.org/10.1038/s41579-025-01200-y.
[5] P. Dutta, S. Das, Curr. Top. Med. Chem. 16 (2016) 99–129, https://doi.org/10.2174/1568026615666150703121819.
[6] C. Wang, T. Hong, P. Cui, J. Wang, J. Xia, Adv. Drug Deliv. Rev. 175 (2021) 113818, https://doi.org/10.1016/j.addr.2021.05.028.
[7] M.D. Seo, H.S. Won, J.H. Kim, T. Mishig-Ochir, B.J. Lee, Molecules 17 (2012) 12276–12286, https://doi.org/10.3390/molecules171012276.
[8] J.M. Sierra, M. Viñas, Expet Opin. Drug Discov. 16 (2021) 601–604, https://doi.org/10.1080/17460441.2021.1892072.
[9] A. Di Donato, M. Tortorella, A. Campanile, L. Rumpel, A. Leone, L. Bosso, A. Petraccone, R. Lombardi, P. Winter, R. Del Vecchio, Oliv, Arch. Biochem. Biophys. 771 (2025) 110526, https://doi.org/10.1016/j.abb.2025.110526.
[10] H. Ma, L. Yang, Z. Tian, L. Zhu, J. Peng, P. Fu, J. Xiu, G. Guo, Int. Microbiol. 26 (2023) 81–90, https://doi.org/10.1007/s10123-022-00274-5.
[11] H. Ma, X. Zhao, L. Yang, S. Pu, P. Fu, J. Peng, N. Yang, G. Guo, Infect. Drug Resist. (2020) 2509–2520, https://doi.org/10.2147/IDR.S250278.
[12] M. El-Fateh, A. Chatterjee, X. Zhao, Int. J. Antimicrob. Agents 63 (2024) 107083, https://doi.org/10.1016/j.ijantimicag.2024.107083.
[13] E. Rai, R. Ferrão, P. Palma, T. Patricio, P. Parreira, E. Anes, C. Tonda-Turo, M. C. Martins, N. Alves, L. Ferreira, J. Mater. Chem. B 10 (2022) 2384–2429, https://doi.org/10.1039/D1TB02617H.
[14] C. Hanna, Y.O. Hermant, P.W. Harris, M.A. Brimble, Acc. Chem. Res. 54 (2021) 1878–1890, https://doi.org/10.1021/acs.accounts.0c00841.
[15] S. Moradi, W.M. Hussein, P. Varamini, P. Simerska, I. Toth, Chem. Sci. 7 (2016) 2492–2500, https://doi.org/10.1039/C5SC04392A.
[16] S.B. Rezende, K.G. Oshiro, N.G. Júnior, O.L. Franco, M.H. Cardoso, Chem. Commun. 57 (2021) 11578–11590, https://doi.org/10.1039/D1CC03793E.
[17] R. Bellavita, S. Braccia, S. Galdiero, A. Falanga, Pharm. Times 16 (2023) 439, https://doi.org/10.3390/ph16030439.
[18] N.G. Bednarska, B.W. Wren, S.J. Willcocks, Drug Discov. Today 22 (2017) 919–926, https://doi.org/10.1016/j.drudis.2017.02.001.
[19] X. Li, Y. Ding, J. Xue, Y. Fu, F. Yan, N. Song, H. Hu, W. Cong, Z. Lu, Y. Li, J. Med. Chem. 68 (2025) 4511–4526, https://doi.org/10.1021/acs.jmedchem.4c02564.

[20] M. Wormald, E. Wooten, R. Bazzo, C. Edge, A. Feinstein, T. Rademacher, R. Dwek, Eur. J. Biochem. 198 (1991) 131–139, https://doi.org/10.1111/j.1432-1033.1991.tb15995.x.
[21] J. Lommerse, L. Kroon-Batenburg, J. Kroon, J. Kamerling, J. Vliegenthart, J. Biomol. NMR 6 (1995) 79–94, https://doi.org/10.1007/BF00417494.
[22] S.E. O'Connor, B. Imperiali, Chem. Biol. 5 (1998) 427–437, https://doi.org/10.1016/S1074-5521(98)90159-4, 31.
[23] M.R. Wormald, R.A. Dwek, Structure 7 (1999) R155–R160, https://doi.org/10.1016/s0969-2126(99)80095-1.
[24] J. Wątły, S. Potocki, M. Rowińska-Żyrek, Chem. Eur J. 22 (2016) 15992–16010, https://doi.org/10.1002/chem.201602376.
[25] A. Som, L. Yang, G.C.L. Wong, G.N. Tew, J. Am. Chem. Soc. 131 (2009) 15102–15103, https://doi.org/10.1021/ja9067063.
[26] L. Falcigno, S. Braccia, R. Bellavita, G. D'Auria, A. Falanga, S. Galdiero, Front. Drug Discov. 4 (2024) 1440378, https://doi.org/10.3389/fddsv.2024.1440378.
[27] M. Sadredinamin, F. Mehrnejad, P. Hosseini, F. Doustdar, Novel Biomed. 4 (2016) 70–76, https://doi.org/10.22037/nbm.v4i2.9158.
[28] P. Méndez-Samperio, Peptides 3 (2010) 1791–1798, https://doi.org/10.1016/j.peptides.2010.06.016.
[29] G. Kilari, J. Tran, G.A. Blyth, E.R. Cobo, Biochim. Biophys. Acta Biomembr. 1867 (2025) 184410, https://doi.org/10.1016/j.bbamem.2025.184410.
[30] R. Bucki, K. Leszczyńska, A. Namiot, W. Sokołowski, Arch. Immunol. Ther. Exp. 58 (2010) 15–25, https://doi.org/10.1007/s00005-009-0057-2.
[31] M.G. Scott, D.J. Davidson, M.R. Gold, D. Bowdish, R.E.W. Hancock, J. Immunol. 169 (2002) 3883–3891, https://doi.org/10.4049/jimmunol.169.7.3883.
[32] O.E. Voronko, V.A. Khotina, D.A. Kashirskikh, A.A. Lee, V.A. Gasanov, Int. J. Mol. Sci. 26 (2025) 8103, https://doi.org/10.3390/ijms26168103.
[33] Y. Yuan, J. Li, G. Wei, Z. Shen, B. Li, J. Wu, J. Liu, ACS Biomater. Sci. Eng. 11 (2025) 3145–3164, https://doi.org/10.1021/acsbiomaterials.4c02029.
[34] H. Shi, P. Shu, Z. Wang, C. Meng, R. Yu, Y. Xu, C. Li, Comput. Methods Biomech. Biomed. Eng. (2025) 1–14, https://doi.org/10.1080/10255842.2025.2477218.
[35] R. Ghasemi, A. Taji, H. Norouzi, M. Koleini, A. Mosadegh, H. Heidari, Probiotics Antimicrob. Proteins (2025), https://doi.org/10.1007/s12602-025-10730-z. Springer.
[36] J.W. Larrick, M. Hirata, R.F. Balint, J. Lee, J. Zhong, S.C. Wright, Infect. Immun. 63 (1995) 1291–1297, https://doi.org/10.1128/iai.63.4.1291-1297.1995.
[37] M.J. Nell, G.S. Tjabringa, A.R. Wafelman, R. Verrijk, P.S. Hiemstra, J.W. Drijfhout, J.J. Grote, Peptides 27 (2006) 649–660, https://doi.org/10.1016/j.peptides.2005.09.016.
[38] J. Brzeski, D. Wyrzykowski, A. Chylewska, M. Makowski, A.M. Papini, J. Makowska, J. Phys. Chem. B 126 (2022) 6911–6921, https://doi.org/10.1021/acs.jpcb.2c05200.
[39] J. Makowska, D. Wyrzykowski, E. Kamysz, A. Tesmar, W. Kamysz, L. Chmurzyński, J. Therm. Anal. Calorim. 138 (2019) 4523–4529, https://doi.org/10.1007/s10973-019-08310-9.
[40] M. D'Accolti, D. Bellotti, E. Dzień, C. Leonetti, S. Leveraro, V. Albanese, E. Marzola, R. Guerrini, E. Caselli, M. Rowińska-Żyrek, M. Remelli, Sci. Rep. 25 (2023) 18228, https://doi.org/10.1038/s41598-023-45437-0.
[41] F. Nuti Paolini, M. de la Cruz PozoCarrero, F. Barbetti, B. Kolesinska, Z. Kaminski, M. Chelli, A.M. Papini, Tetrahedron Lett. 48 (2007) 2901–2904, https://doi.org/10.1016/j.tetlet.2007.02.087.
[42] X.L. Wei, J.B. Xiao, Y. Wang, Y. Bai, Spectrochim. Acta 75 (2010) 299–304, https://doi.org/10.1016/j.saa.2009.10.027.
[43] E. Sacco, S.J. Abraham, A. Palmioli, G. Damore, A. Bargna, E. Mazzoleni, V. Gaponenko, M. Vanoni, F. Peri, Medchemcomm 2 (2011) 396–401, https://doi.org/10.1039/C0MD00264J.
[44] D.A. Case, K. Belfon, I.Y. Ben-Shalom, S.R. Brozell, D.S. Cerutti, T.E. Cheatham, III, V.W.D. Cruzeiro, T.A. Darden, R.E. Duke, G. Giambasu, M.K. Gilson, H. Gohlke, A. W. Goetz,R Harris, S. Izadi, S.A. Izmailov, K. Kasavajhala, A. Kovalenko, R. Krasny, T. Kurtzman, T.S. Lee, S. LeGrand, P. Li, C. Lin, J. Liu, T. Luchko, R. Luo, V. Man, K. M. Merz, Y. Miao, O. Mikhailovskii, G. Monard, H. Nguyen, A. Onufriev, F. Pan, S. Pantano, R. Qi, D.R. Roe, A. Roitberg, C. Sagui, S. Schott-Verdugo, J. Shen, C.L. Simmerling, N.R. Skrynnikov, J. Smith, J. Swails, R.C. Walker, J. Wang, L. Wilson, R.M. Wolf, X. Wu, Y. Xiong, Y. Xue, D.M. York, P.A. Kollman, AMBER 2020, University of California, San Francisco.
[45] T. Dudev, C. Lim, Acc. Chem. Res. 40 (2007) 85–93, https://doi.org/10.1021/ar068181i.
[46] E. Grimsey, D.W.P. Collis, R. Mikut, K. Hilpert, Biochim. Biophys. Acta Biomembr. 1 (2020) 183195, https://doi.org/10.1016/j.bbamem.2020.183195.
[47] D. Łoboda, H. Kozłowski, M. Rowińska-Żyrek, New J. Chem. 42 (2018) 7560–7568, https://doi.org/10.1039/C7NJ04709F.
[48] J.L. Alexander, Z. Thompson, J.A. Cowan, ACS Chem. Biol. 13 (2018) 844–853, https://doi.org/10.1021/acschembio.7b00989.
[49] M.D. Libardo, S. Nagella, A. Lugo, S. Pierce, A.M. Angeles-Boza, Biochem. Biophys. Res. Commun. 2 (2015) 446–451, https://doi.org/10.1016/j.bbrc.2014.11.104.
[50] L.A. Salvador, M. Elofsson, J. Kihlberg, Tetrahedron 51 (1995) 5643–5656, https://doi.org/10.1016/0040-4020(95)00224-V.
[51] F. Nuti, F.R. Fernandez, G. Sabatino G, E. Peroni, B. Mulinacci, I. Paolini, M. Di Pisa, C. Tiberi, F. Lolli, M. Petruzzo, R. Lanzillo, V. Brescia Morra, P. Rovero, A. M. Papini, Brain Sci. 10 (2020) 453, https://doi.org/10.3390/brainsci10070453.
[52] M. Quagliata, F. Nuti, F. Real-Fernandez, K. Kirilova Kirilova, F. Santoro, A. Carotenuto, A.M. Papini, P. Rovero, J. Pept. Sci. 29 (2023) e3475, https://doi.org/10.1002/psc.3475.
[53] K. Sikora, M. Bauer, S. Bartoszewska, D. Neubauer, W. Kamysz, Biomolecules 13 (2023) 172, https://doi.org/10.3390/biom13010172.
[54] J.A. Maier, C. Martinez, K. Kasavajhala, L. Wickstrom, K.E. Hauser, C. Simmerling, J. Chem. Theor. Comput. 11 (2015) 3696–3713, https://doi.org/10.1021/acs.jctc.5b00255.
[55] K.N. Kirschner, A.B. Yongye, S.M. Tschampel, J. González-Outeiriño, C.R. Daniels, B.L. Foley, R.J. Woods, J. Comput. Chem. 4 (2008) 622–655, https://doi.org/10.1002/jcc.20820.
[56] W. Humphrey, A. Dalke, K. Schulten, J. Mol. Graph. 14 (1996) 33–38, https://doi.org/10.1016/0263-7855(96)00018-5.